J. Fluid Mech. (1987), *vol.* 176, *pp.* 403–417
Printed in Great Britain

Nonlinear oscillatory convection

By R. M. CLEVER AND F. H. BUSSE
Institut für Physik, Universität Bayreuth, 8580 Bayreuth, West-Germany

(Received 6 March 1986 and in revised form 14 August 1986)

A numerical analysis has been performed of three-dimensional time-dependent solutions which bifurcate supercritically from two-dimensional convection-roll solutions at the onset of the oscillatory instability. The bifurcating solutions describe a periodic shifting forward and backward of the convection rolls and lead to a strong deformation of the rolls as the Rayleigh number increases. Since the bifurcating solution is stable in the form of a travelling wave, the computational expense can be reduced by assuming a moving coordinate. Travelling-wave solutions have been computed in the case of rigid boundaries as a function of the Prandtl number and of the two basic wavenumbers α_x, α_y of the problem. The onset of oscillations reduces the heat transport in comparison with that of two-dimensional rolls because the occupation of a new degree of freedom of motion by the oscillation reduces the energy of the heat-transporting component of convection. A limited stability analysis of finite-amplitude travelling waves has been performed and the onset of an asymmetric mode of oscillations is determined as a function of the parameters of the problem. This mode appears to be identical with a mode that was observed in the numerical simulations of Lipps (1976) and McLaughlin & Orszag (1982).

1. Introduction

The onset of oscillatory convection has long received special attention among workers in the field of thermal convection because it represents an important step in the evolution towards turbulence. Detailed observations of oscillatory convection in low-Prandtl-number fluids have been made by Willis & Deardorff (1970) who clearly demonstrated that the oscillations consist of waves propagating along the axis of convection rolls. A theory of such waves was derived by Busse (1972) in the case of stress-free boundaries and has been extended to the case of rigid boundaries by Clever & Busse (1974, hereinafter referred to as I). While the onset of the oscillatory instability has been well understood on the basis of these theories and found to be in good agreement with the experimental data, the finite-amplitude properties are less well understood. The experimental observations indicate either a slight increase in the dependence on the Rayleigh number of the slope of the convective heat transport in air (Krishnamurti 1973) or no change at all (Brown 1973). A decrease in the slope has been observed in recent experiments on the onset of oscillations in liquid helium (Maeno, Haucke & Wheatley 1985). Other observations made in mercury suggest the opposite behaviour (Fauve & Libchaber 1981). Different Prandtl numbers and varying aspect ratios of the convection layers are probably responsible for most of the variations in the reported results.

In this paper nonlinear properties of oscillatory convection are investigated for different Prandtl numbers as a function of wavenumber and Rayleigh number. In this respect the present analysis complements earlier numerical investigations by

Lipps (1976), Grötzbach (1982), and McLaughlin & Orszag (1982) who focused their attention on particular values of these parameters. In particular, convection in air has been assumed throughout the earlier work, while the present paper emphasizes the Prandtl-number dependence. As will be shown, oscillatory convection appears to have a much more profound influence on the heat transport and other properties at Prandtl numbers lower than that of air. Other features of oscillatory convection also exhibit a strong dependence on the Prandtl number. While the present work was being completed the authors become aware of the work by Meneguzzi *et al.* (1985) which also presents numerical simulations of convection at low Prandtl numbers. The latter work complements the present analysis in several ways since it emphasizes stress-free boundaries which cause significant changes from the case of rigid boundaries and since it also investigates transient effects which are not studied in the present paper.

The paper starts with an exposition of the mathematical method of analysis in §2 and proceeds with a discussion of travelling waves in §3. The stability of these waves is investigated in §4. Some results for asymmetric travelling waves which replace the symmetric waves are also presented in §4. Concluding remarks are offered in §5.

2. Mathematical formulation of the problem

We consider convection in a horizontal fluid layer heated from below. Using the thickness d of the layer as lengthscale, d^2/κ as timescale, and $\kappa\nu/d^3\gamma g$ as the scale of the temperature, we can write the basic equation in dimensionless form. The symbols κ, ν, γ, g refer to the thermal diffusivity, the kinematic viscosity, the coefficient of thermal expansion, and gravity respectively. The Boussinesq approximation will be assumed, such that the velocity field is described by a solenoidal vector field. A general representation of those vector fields is given by

$$\boldsymbol{v} = \boldsymbol{\nabla}\times(\boldsymbol{\nabla}\times\boldsymbol{k}\phi)+\boldsymbol{\nabla}\times\boldsymbol{k}\psi \equiv \boldsymbol{\delta}\phi+\boldsymbol{\varepsilon}\psi, \tag{2.1}$$

where $\boldsymbol{k}$ is a unit vector. We choose $\boldsymbol{k}$ in the vertical direction parallel to the z-axis of a Cartesian system of coordinates with the origin on the median plane of the layer. The equations for the scalar functions ϕ and ψ are obtained from the z-components of the (curl)^2 and the curl of the equations of motion,

$$\nabla^4 \Delta_2 \phi = P^{-1}\left\{\boldsymbol{\delta}\cdot[(\boldsymbol{\delta}\phi+\boldsymbol{\varepsilon}\psi)\cdot\boldsymbol{\nabla}(\boldsymbol{\delta}\phi+\boldsymbol{\varepsilon}\psi)]+\frac{\partial}{\partial t}\nabla^2\Delta_2\phi\right\}, \tag{2.2a}$$

$$\nabla^2 \Delta_2 \psi = P^{-1}\left\{\boldsymbol{\varepsilon}\cdot[(\boldsymbol{\delta}\psi+\boldsymbol{\varepsilon}\psi)\cdot\boldsymbol{\nabla}(\boldsymbol{\delta}\phi+\boldsymbol{\varepsilon}\psi)]+\frac{\partial}{\partial t}\Delta_2\psi\right\}, \tag{2.2b}$$

where Δ_2 denotes the two-dimensional Laplacian, $\Delta_2 = \nabla^2-(\boldsymbol{k}\cdot\boldsymbol{\nabla})^2$. The heat equation for the dimensionless deviation θ of the temperature distribution from the static state of the fluid layer is given by

$$\nabla^2\theta - R\Delta_2\phi = (\boldsymbol{\delta}\phi+\boldsymbol{\varepsilon}\psi)\cdot\boldsymbol{\nabla}\theta+\frac{\partial}{\partial t}\theta, \tag{2.2c}$$

The Rayleigh number R and the Prandtl number P are defined in the usual way,

$$R \equiv \frac{\gamma g(T_2-T_1)\,d^3}{\kappa\nu}, \quad P = \nu/\kappa,$$

where T_1 and T_2 are the temperatures at the upper and lower boundaries of the layer.

Equations (2.2), together with the boundary conditions

$$\phi = \frac{\partial}{\partial z}\phi = \psi = \theta = 0 \quad \text{at } z = \pm\tfrac{1}{2}, \tag{2.3}$$

can be solved by the Galerkin technique. The dependent variables are expanded into complete systems of functions satisfying the boundary conditions (2.3). In the simplest case of travelling-wave solutions, time-independent coefficients can be assumed,

$$\phi = \sum_{\beta,\lambda,\nu} [\hat{a}_{\beta\lambda\nu}\cos\beta\alpha_x(x-ct) + a_{\beta\lambda\nu}\sin\beta\alpha_x(x-ct)] \begin{Bmatrix}\sin\lambda\alpha_y y\\ \cos\lambda\alpha_y y\end{Bmatrix} g_\nu(z)$$

$$\equiv \sum_{\beta,\lambda,\nu} [\hat{a}_{\beta\lambda\nu}\hat{\phi}_{\beta\lambda\nu} + a_{\beta\lambda\nu}\phi_{\beta\eta\nu}], \tag{2.4a}$$

$$\theta = \sum_{\beta,\lambda,\nu} [\hat{b}_{\beta\lambda\nu}\cos\beta\alpha_x(x-ct) + b_{\beta\lambda\nu}\sin\beta\alpha_x(x-ct)] \begin{Bmatrix}\sin\lambda\alpha_y y\\ \cos\lambda\alpha_y y\end{Bmatrix} \sin\nu\pi(z+\tfrac{1}{2})$$

$$\equiv \sum_{\beta,\lambda,\nu} [\hat{b}_{\beta\lambda\nu}\hat{\theta}_{\beta\lambda\nu} + b_{\beta\lambda\nu}\theta_{\beta\lambda\nu}], \tag{2.4b}$$

$$\psi = \sum_{\beta,\lambda,\nu} [\hat{c}_{\beta\lambda\nu}\cos\beta\alpha_x(x-ct) + c_{\beta\lambda\nu}\sin\beta\alpha_x(x-ct)] \begin{Bmatrix}\sin\lambda\alpha_y y\\ \cos\lambda\alpha_y y\end{Bmatrix} \sin\nu\pi(z+\tfrac{1}{2})$$

$$\equiv \sum_{\beta,\lambda,\nu} [\hat{c}_{\beta\lambda\nu}\hat{\psi}_{\beta\lambda\nu} + c_{\beta\lambda\nu}\psi_{\beta\lambda\nu}]. \tag{2.4c}$$

The indices β and λ run through all non-negative integers while ν runs through all positive integers. The functions $g_\nu(z)$ were introduced by Chandrasekhar (1961, p. 635) and have also been defined in equation (11a) of I. In the wavy brackets of (2.4) the upper functions must be chosen for odd integers β, the lower functions for even β. In addition all coefficients with odd $\lambda+\nu$ may be dropped, if attention is restricted to travelling waves bifurcating in the form of the oscillatory instability from the solution describing steady rolls with the axis in the x-direction. In the case of an infinitesimal deviation from the steady-roll solution all terms with $\beta \geqslant 2$ may be dropped. Terms corresponding to $\beta = 1$ represent the eigenvector of the oscillatory instability where the phase of the disturbance has been fixed such that all terms proportional to $\cos\alpha_x(x-ct)$ vanish. As the amplitude of the disturbance increases terms symmetric in y and proportional to $\cos 2\alpha_x(x-ct)$ are generated. Thus the higher-order terms continue to obey the symmetry property mentioned above.

We obtain algebraic equations for the coefficients $\hat{a}_{\beta\lambda\nu}, a_{\beta\lambda\nu}, \hat{b}_{\beta\lambda\nu}, \ldots$ by multiplying (2.2) with the functions $\hat{\phi}_{\beta\lambda\nu}, \phi_{\beta\lambda\nu}, \hat{\theta}_{\beta\lambda\nu}, \ldots$ and averaging the result over the fluid layer. The resulting equations cannot be given explicitly here; they are of the same form except for additional terms as equations (2.12) of Busse & Frick (1985). In order to solve the equations numerically a truncation scheme must be introduced. Extending the procedure used in I we neglect all coefficients and equations with indices satisfying

$$\beta+\lambda+\nu > N_{\mathrm{T}}. \tag{2.5}$$

For given values of R, α_x and α_y the algebraic equations for the coefficients $a_{\beta\lambda\nu}$, etc. are solved by a Newton–Raphson iteration method. Since the phase of the travelling waves is arbitrary, we fix it by prescribing $a_{111} = 0$. The corresponding equation obtained by the multiplication of (2.2a) with $\phi_{\beta\lambda\nu}$ serves for the determination of the phase velocity c.

The stability of the stationary-travelling-wave solutions can be investigated by superimposing infinitesimal disturbances $\tilde{\phi}, \tilde{\theta}, \tilde{\psi}$ onto the stationary solutions. Since experimental results and previous numerical computations indicate that the instability of the travelling-wave solution does not change the horizontal wavelengths, we restrict attention to disturbances of the form (2.4), where the coefficient $\hat{a}_{\beta\lambda\nu}$ is replaced by $\hat{\hat{a}}_{\beta\lambda\nu} \exp\{\sigma t\}$ with analogous replacements for the other coefficients. No restrictions on the indices β, λ, ν are imposed. But owing to the symmetry of the stationary solution the disturbances separate into four classes; the index β for the functions in the wavy bracket can either be of the same parity as for the stationary solution or of the opposite one. Independently the sum of the indices λ and ν can be either even or odd. This subdivision of the stability analysis greatly reduces the computational expanses.

Once the strongest growing disturbances among the four classes has been determined, its evolution to finite amplitude can be followed by a forward integration in time. For this purpose the coefficients in the representation (2.4) are assumed to be functions of time and the implicit dependence on time in the form of the moving coordinate $x - ct$ is dropped,

$$\phi = \sum_{\beta,\lambda,\nu} [\hat{a}_{\beta\lambda\nu}(t) \cos\beta\alpha_x x + a_{\beta\lambda\nu}(t) \sin\beta\alpha_x x] \begin{Bmatrix} \sin\lambda\alpha_y y \\ \cos\lambda\alpha_y y \end{Bmatrix} g_\nu(z), \tag{2.6a}$$

$$\theta = \sum_{\beta,\lambda,\nu} [\hat{b}_{\beta\lambda\nu}(t) \cos\beta\alpha_x x + b_{\beta\lambda\nu}(t) \sin\beta\alpha_x x] \begin{Bmatrix} \sin\lambda\alpha_y y \\ \cos\lambda\alpha_y y \end{Bmatrix} \sin\nu\pi(z+\tfrac{1}{2}), \tag{2.6b}$$

$$\psi = \sum_{\beta,\lambda,\nu} [\hat{c}_{\beta\lambda\nu}(t) \cos\beta\alpha_x x + c_{\beta\lambda\nu}(t) \sin\beta\alpha_x x] \begin{Bmatrix} \sin\lambda\alpha_y y \\ \cos\lambda\alpha_y y \end{Bmatrix} \sin\nu\pi(z+\tfrac{1}{2}). \tag{2.6c}$$

Since among the four classes of disturbances only the class with odd $\lambda + \nu$ and a parity of β opposite to that of the stationary solution gives rise to instability, only the case where the upper function in the wavy bracket corresponds to odd $\beta + \lambda + \nu$ and the lower bracket corresponds to even $\beta + \lambda + \nu$ will be considered. A semi-implicit Crank–Nicholson scheme was used for the integration in time of the system of equations for the coefficients $\hat{a}_{\beta\lambda\nu}(t)$, etc., which are derived from the basic equations in the same way as the algebraic equations for the stationary solution.

In principle the integration in time should also permit the generation of solutions in the form of standing waves. But it was observed that even with a suitable choice of initial condition the integration in time always led to travelling-wave solutions. This is not surprising since it is known from other studies that the standing-wave solutions are usually unstable with respect to travelling-wave disturbances. No special effort was therefore expanded to obtain standing-wave solutions.

3. Travelling waves

One of the characteristic properties of the oscillatory instability of convection rolls is the introduction of a toroidal velocity component connected with a vertical component of vorticity. Figure 1 describes the growth of the kinetic energy associated with the toroidal component of the velocity field,

$$E_{\text{tor}} \equiv \tfrac{1}{2}\langle |\nabla \times k\psi|^2 \rangle = -\tfrac{1}{2}\langle \psi \Delta_2 \psi \rangle, \tag{3.1}$$

where the angular brackets denote the average over the fluid layer. The data actually computed have been given in the figure to indicate their density. It is of interest to

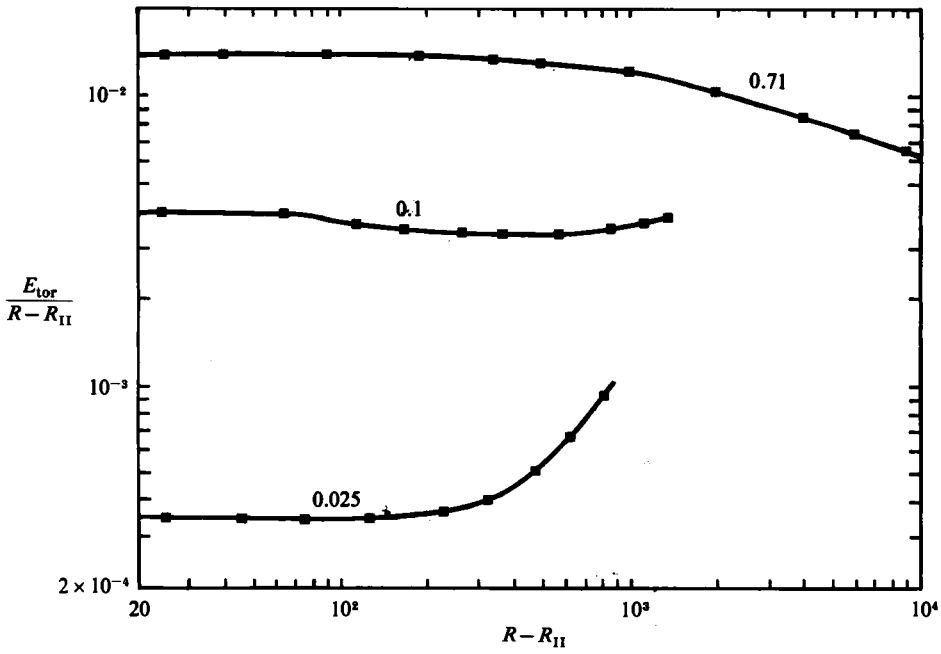

FIGURE 1. Dependence of the kinetic energy E_{tor} of the toroidal component of motion on the supercritical Rayleigh number $R-R_{II}$ for the indicated values of the Prandtl number P with $(\alpha_x, \alpha_y) = (2.3, 2.2)$ for $P = 0.71$, $(\alpha_x, \alpha_y) = (2.2, 2.6)$ for $P = 0.1$, $(\alpha_x, \alpha_y) = (2.2, 2.9)$ for $P = 0.025$.

see that E_{tor} exhibits a linear growth as a function of the supercritical Rayleigh number $R-R_{II}$, over an extended range of the latter parameter except in the case of mercury. Here R_{II} denotes the Rayleigh number for the onset of the oscillatory instability. The wavenumbers α_x, α_y that have been selected for the curves correspond to the range of observed wavenumbers (Willis & Deardorff 1970) and to the range where the oscillatory instability defines the boundary of stable rolls as shown in Clever & Busse (1978). When the dependence on the wavenumber α_x of the travelling wave is analysed it is found that for air, $P = 0.71$, E_{tor} increases with increasing α_x at a constant value of $R-R_{II}$ while at lower Prandtl number E_{tor} decreases. This difference in the dependence of E_{tor} may be a reflection of the Prandtl-number dependence of R_{II}. In the case of air the Rayleigh number R_{II} for onset of oscillations is large and higher wavenumbers are more easily excited than in the case of the low values of R_{II} obtained in low-Prandtl-number fluids.

Figures 2 and 3 show typical variations of the shape of the travelling waves as a function of the Rayleigh number. Again it appears that higher harmonics are more easily excited in the case of air than in the case of the lower Prandtl number $P = 0.1$. A typical feature of the low-Prandtl-number case appears to be the evolution with increasing Rayleigh number from the sinusoidal wave form to a zigzag wave form. But the amplitude of the distortion of the original rolls does not increase much after it has reached about half a wavelength. The increase in kinetic energy of the toroidal velocity component does not manifest itself primarily in a growing amplitude of the wave once $(R-R_{II})/R_{II}$ has reached a level of the order 0.1–0.2. Instead the growing toroidal component of motion appears to be associated with the growth of higher harmonics of the wave and with an increase in the frequency of oscillations. The latter

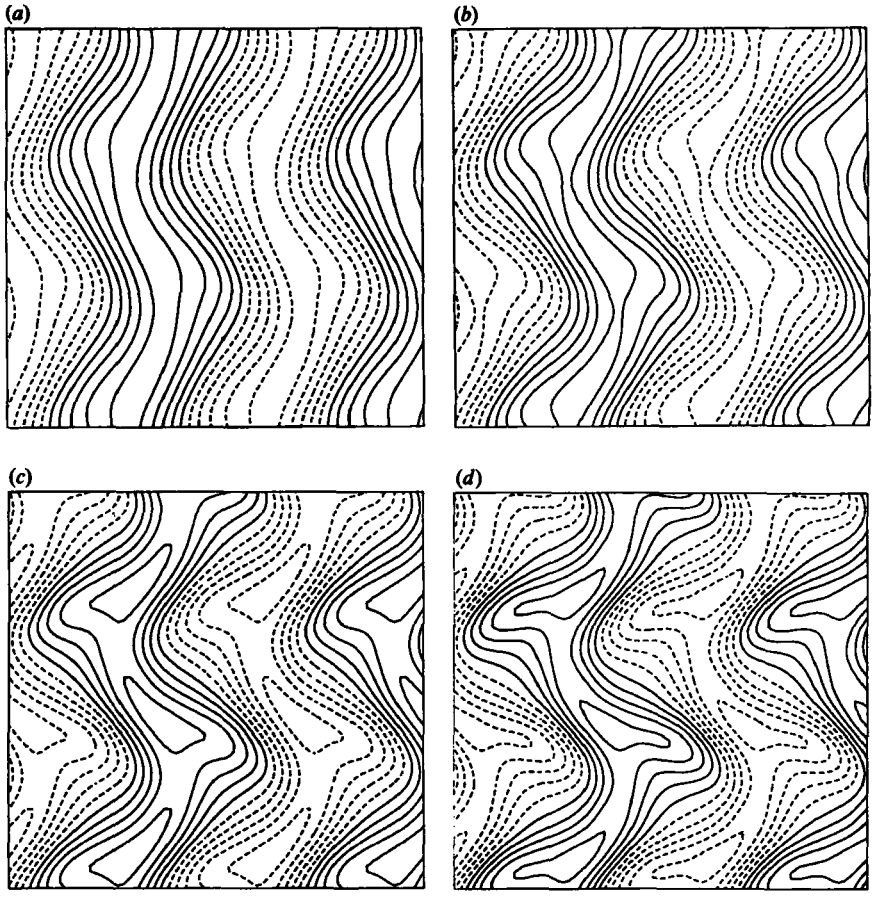

FIGURE 2. Lines of constant vertical velocity in the plane $z = 0$ for travelling-wave convection with $\alpha_x = 2.3$, $\alpha_y = 2.2$, $P = 0.71$. (*a*) $R = 6.5 \times 10^3$; (*b*) 7×10^3; (*c*) 8×10^3; (*d*) 10^4. The truncation parameter $N_T = 9$ has been used. The waves travel in the downward direction.

effect is most pronounced in low-Prandtl-number fluids as shown in figure 4, while the former feature is more pronounced at a higher Prandtl number as suggested by figure 2.

The frequency of oscillation actually decreases first after the onset of the oscillatory instability in low-Prandtl-number fluids unless the wavenumber of the convection rolls is rather low. This phenomena is evident in figure 4 and must be attributed to the concurrent decrease of the circulation velocity of rolls. This decrease is also evident in the decrease of the kinetic energy of the poloidal component of motion shown in figure 5. Note that the quantity

$$E_{\rm pol}/(R-R_c) \equiv \tfrac{1}{2}\langle|\nabla \times (\nabla \times k\phi)|^2\rangle/(R-R_{\rm c}), \tag{3.2}$$

has been plotted in order to emphasize the dramatic change that occurs after the onset of travelling waves. But $E_{\rm pol}$ itself also decreases with increasing R near $R = R_{\rm II}$ at least for the wavenumbers $\alpha_y = 2.2$ and 2.5. The fact that the change in the kinetic energy of the poloidal component of motion is less dramatic for lower wavenumbers of the convection rolls can be attributed to the onset of the oscillatory instability increasing the effective wavenumber of convection and thereby increasing the

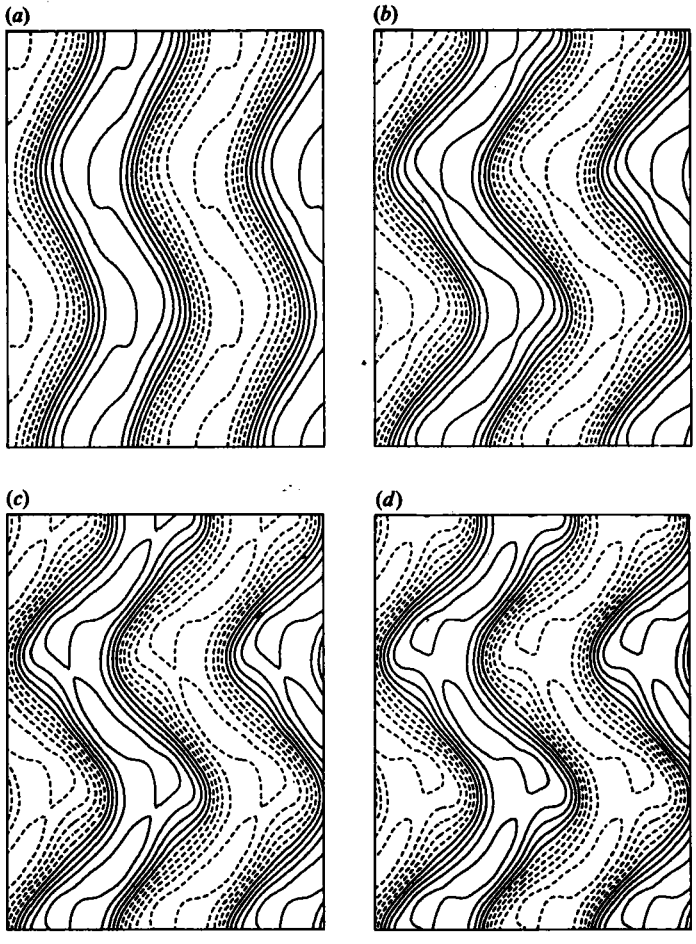

FIGURE 3. Same as figure 2, but for $P = 0.025$, $\alpha_x = 2.2$, $\alpha_y = 2.9$. (*a*) $R = 2000$; (*b*) 2200; (*c*) 2350; (*d*) 2500.

efficiency of convection in converting available potential energy into mechanical energy of motion. For wavenumbers closer to the critical value this effect is much smaller.

It is not surprising that the kinetic energy of the poloidal component of motion grows less rapidly or even decreases after a new degree of freedom of motion becomes occupied. Less expected is the property that the total kinetic energy of the travelling waves is lower than that of the steady rolls. This fact holds for the low-Prandtl-number cases, though not for air for which a slight increase in the total kinetic energy can be seen in table 1. In table 1 the numerical values of the Nusselt number have also been listed. The Nusselt number describes the ratio between the heat transport with and without convection and is given by

$$Nu = 1 - R^{-1} \sum_n n\pi \hat{b}_{00n}. \tag{3.3}$$

For $P = 0.71$ the Nusselt number for convection rolls and travelling-wave convection is so close that the difference is not easily discerned in a graphical representation. In fact, the numerical differences for different truncation numbers N_T tend to

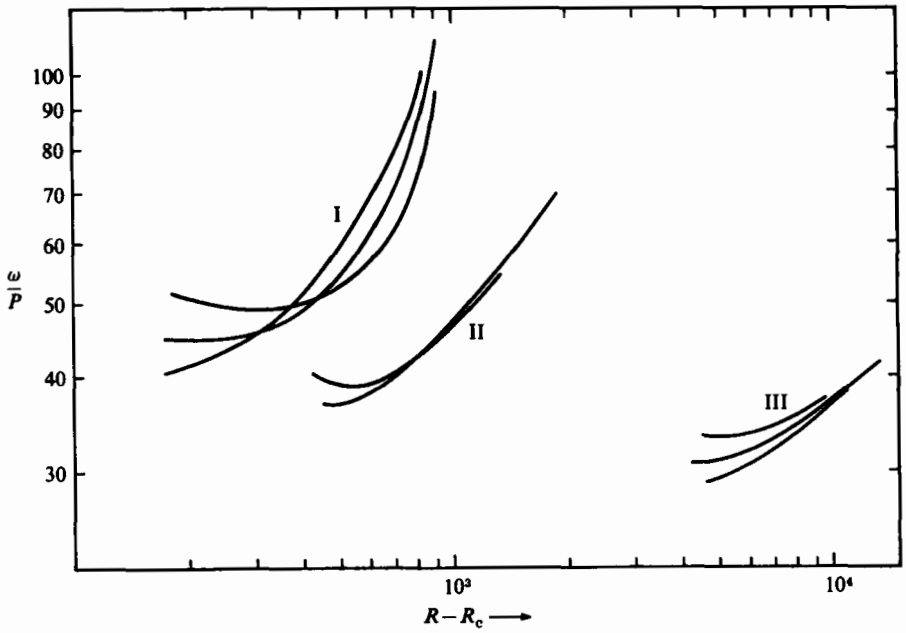

FIGURE 4. The frequency ω of the symmetric travelling waves as a function of $R-R_c$ for the Prandtl numbers $P = 0.025$ (I), $P = 0.1$ (II), $P = 0.71$ (III). The wavenumber α_y assumes the values 2.9 (I), 2.6 (II), 2.2 (III). The different curves correspond to $\alpha_x = 1.9$, 2.2, 2.5 (I), $\alpha_x = 1.9$, 2.2 (II), and $\alpha_x = 2.0$, 2.3, 2.6 (III). At the low-Rayleigh-number end the frequency increases monotonically with α_x in each case.

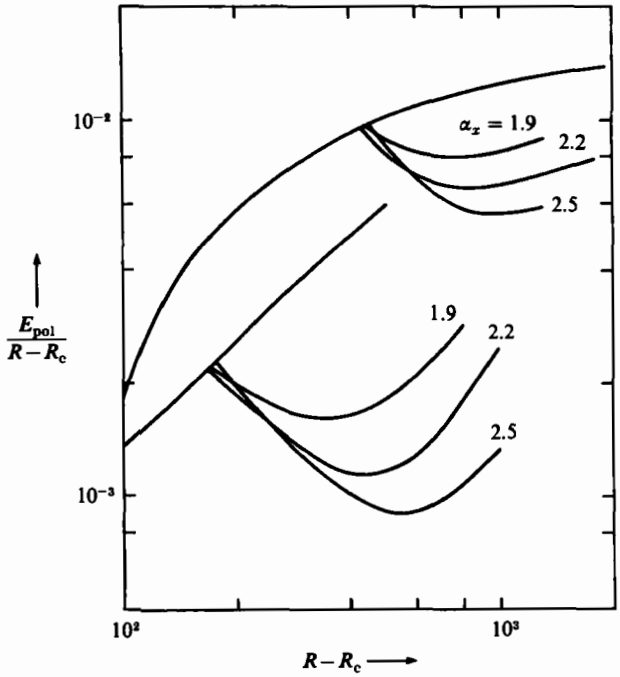

FIGURE 5. Kinetic energy E_{pol} of the poloidal component of motion for two-dimensional rolls and for three-dimensional wave solutions branching off the two-dimensional solution with different values of α_x as indicated. The upper set of curves corresponds to $P = 0.1$, $\alpha_y = 2.6$, the lower one to $P = 0.025$, $\alpha_y = 2.9$.

Rayleigh number R	Nusselt number Nu: 2-Dimensional $\alpha_y = 2.2$, $N_T = 6$	2-Dimensional $\alpha_y = 2.2$, $N_T = 8$	2-Dimensional $\alpha_y = 2.2$, $N_T = 10$	Travelling-wave solution $\alpha_y = 2.2, \alpha_x = 2.3$, $N_T = 7$	Travelling-wave solution $\alpha_y = 2.2, \alpha_x = 2.3$, $N_T = 8$	Travelling-wave solution $\alpha_y = 2.2, \alpha_x = 2.3$, $N_T = 9$	Frequency ω $N_T = 9$†	Kinetic energy: Poloidal, E_{pol}: 2-Dimensional rolls $N_T = 10$	Kinetic energy: Poloidal, E_{pol}: Travelling waves $N_T = 9$†	Kinetic energy: Toroidal, E_{tor} travelling waves $N_T = 9$†
6000	2.1099	2.0949	2.0900	—	—	—	—	81.33	—	—
6050	2.1165	2.1013	2.0963	2.1159	—	—	21.89	82.44	82.04	0.5615
6100	2.1231	2.1076	2.1026	2.1216	—	—	21.90	83.54	82.65	1.258
6500	2.1733	2.1561	2.1505	2.1679	2.1497	2.1496	22.02	92.45	87.89	6.440
7000	2.2316	2.2121	2.2058	2.2240	2.2026	2.2021	22.26	103.7	95.19	11.99
8000	2.3364	2.3122	2.3044	2.3265	2.2988	2.2973	22.97	126.8	111.2	20.70
10000	2.5135	2.4796	2.4684	2.4973	2.4590	2.4541	24.74	174.7	145.8	33.80
12000	2.6631	2.6192	2.6041	2.6381	2.5910	2.5814	26.65	224.7	182.0	44.71
15000	2.8554	2.7967	2.7754	2.8155	2.7556	2.7393	29.48	302.0	237.5	58.90

† $N_T = 7$ for $R = 6050, 6100$.

TABLE 1. Numerical results for $P = 0.71$, convection in air

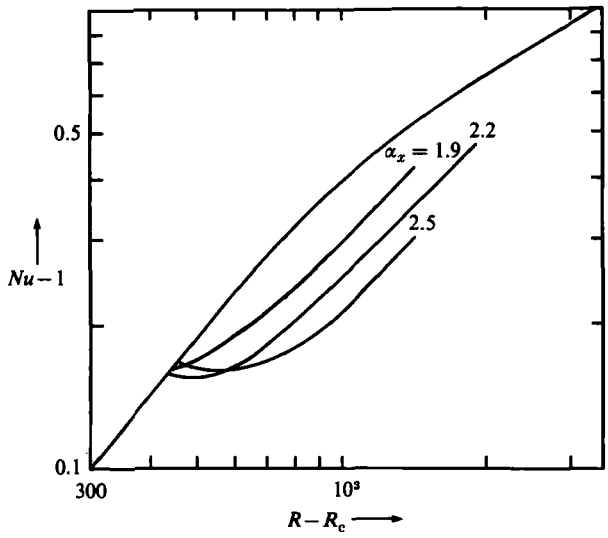

FIGURE 6. Nusselt number Nu as a function of $R-R_c$ for two-dimensional rolls and travelling-wave solutions with $\alpha_x = 1.9, 2.2, 2.5$ (as indicated) in the case $P = 0.1$, $\alpha_y = 2.6$.

overshadow the difference between two- and three-dimensional convection. But the rate of numerical convergence can be estimated from the results for different N_T, and the comparison of values from two-dimensional computations for a given N_T with those from three-dimensional computations at the same N_T should give the most reliable estimate for the ratio of the heat transport. The rate of convergence is usually found to be better for three-dimensional than for two-dimensional computations at the same values of N_T. This property is caused by more rapid increase of the number of modes in the former case.

The onset of oscillatory instability adds a new sink of energy in the form of the dissipation by the toroidal component of motion without providing an additional source of energy since the latter component of motion does not contribute to the work of the buoyancy force. Thus one expects the efficiency of the heat transport to decrease in the evolution of travelling-wave convection from rolls with the same wavenumber α_y. Table 1 shows this effect. The relative small difference between the Nusselt numbers for two- and three-dimensional convection appears to be caused by a compensating effect. Because of the increasing x-dependence of convection with increasing wave amplitude the effective wavenumber of convection is also increased. From the study of two-dimensional convection it is well known that the Nusselt number increases with increasing α_y in the relevant parameter region (see Table 1 of I). This effect thus compensates in part the inefficiency of the heat transport by travelling waves noted above.

In low-Prandtl-number fluids this compensating effect is too weak to be significant. The dramatic change in the Nusselt-number dependence on the Rayleigh number shown in figures 6 and 7 indicates that the onset of oscillatory instability destroys the subtle balance by which the phenomenon of inertial convection is approached in steady rolls (Jones, Moore & Weiss 1976; Clever & Busse 1981). But in connection with the evolution from sinusoidal to zigzagging waves the heat transport recovers and exhibits an even stronger increase with Rayleigh number than that of two-dimensional rolls. The comparison with experimentally measured values in the case

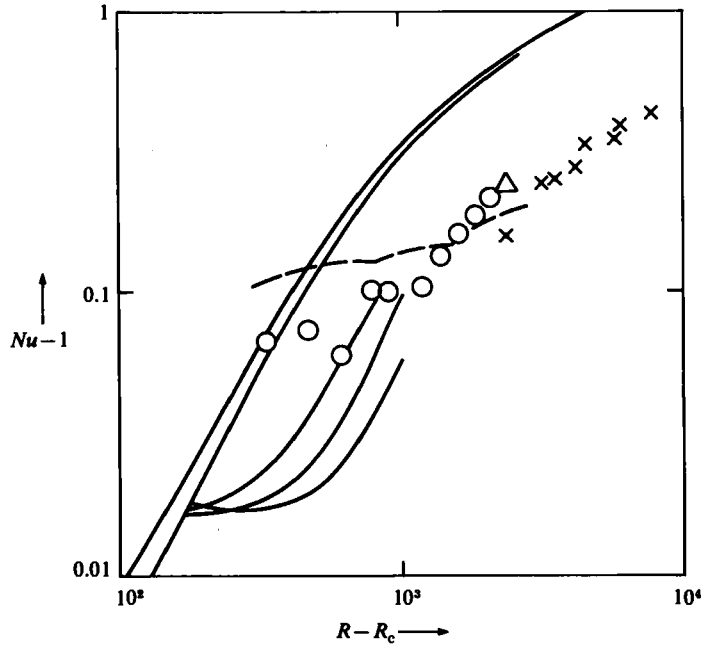

FIGURE 7. Same as figure 6 for $P = 0.025$, $\alpha_y = 2.9$. In addition the Nusselt number for $\alpha_y = 3.117$ has been included (left curve). Experimental results of Krishnamurti (1973), given by the dashed line, and of Rossby (1969) are shown for comparison. In the latter case symbols indicate different layer depths: $d = 0.19$ cm (○; 1.0 cm (×); 1.8 cm (△).

of mercury indicates good agreement. The strong recovery of the heat transport by travelling-wave convection suggests an effect similar to that of inertial convection in steady rolls. In the latter case the curl of the advection term $\boldsymbol{v}\cdot\nabla\boldsymbol{v}$ is minimized by nearly circular streamlines. The zigzag wave pattern with piecewise straight rolls may indicate a balance similar to that for steady rolls.

4. Transition to asymmetric-travelling-wave convection

From the numerical simulations of Lipps (1976) and McLaughlin & Orszag (1982) it is known that the symmetric-travelling-wave solutions discussed in the preceeding section become asymmetric as the Rayleigh number is increased. In this section we investigate this process using a stability analysis and study its dependence on the Prandtl number and other parameters of the problem. As has already been indicated in §2 the stability analysis will be restricted to disturbances with the same horizontal periodicity as that of the symmetric-travelling-wave solution. With this restriction the possible disturbances separate into four classes depending on their symmetry with respect to the stationary travelling waves. When maximum real parts of the growth rate σ are computed as a function of the Rayleigh number, it is found that always the same class of disturbances gives rise to the eigenvalue σ for which the real part σ_r becomes positive first with increasing Rayleigh number R. This class of disturbances is characterized by the property that the parity with respect to the y-dependence is opposite to that of the stationary-travelling-wave solution, i.e. $\sin\lambda\alpha_y y$-terms in the representation for $\tilde{\phi}$ correspond to even indices β, while

	$P = 0.71$, $\alpha_y = 2.2$			$P = 0.1$, $\alpha_y = 2.6$			$P = 0.025$, $\alpha_y = 2.9$		
	$\alpha_x = 2.0$	$\alpha_x = 2.3$	$\alpha_x = 2.6$	$\alpha_x = 1.9$	$\alpha_x = 2.2$	$\alpha_x = 2.5$	$\alpha_x = 1.9$	$\alpha_x = 2.2$	$\alpha_x = 2.5$
R_{III}	11270	9110	7830	2918	2683	2680	2453	2382	2293
σ_{i}	15.95	11.40	8.95	4.015	3.856	4.043	1.061	1.330	1.255

TABLE 2. Rayleigh numbers R_{III} and imaginary parts σ_{i} of growth rates for the onset of asymmetric oscillations ($N_{\mathrm{T}} = 8$)

$\cos \lambda\alpha_y y$-terms correspond to odd β. Concurrently coefficients $\hat{\tilde{a}}_{\beta\lambda\nu}$, $\tilde{a}_{\beta\lambda\nu}$, etc. with even $\lambda + \nu$ vanish for this class of disturbances.

The critical values R_{III} of the Rayleigh number at which asymmetric disturbances first start to grow and the corresponding values of the imaginary part σ_{i} of the growth rate are shown as a function of α_x in table 2. The truncation parameter $N_{\mathrm{T}} = 8$ has been used for these calculations. Some tests carried out with $N_{\mathrm{T}} = 9$ indicate that the results approach the exact results to within a few percent. Evidently waves with short wavelengths are more unstable than those with longer wavelengths. The onset of instability depends primarily on the amplitude of the wave, measured in terms of the distortion of the original rolls. A rough measure for the onset of the asymmetric instability is that the kinetic energy of the toroidal component of motion reaches about one quarter of the kinetic energy of the poloidal component of motion. This fraction is a little less than one quarter in the case of air and a little more in the low-Prandtl-number cases.

The imaginary part σ_{i} of the growth rate σ is comparable with the frequency of the stationary travelling waves. In general σ_{i} is smaller than $\omega_1 \equiv c/\alpha_x$, but it approaches this value in the case of mercury for higher values of α_x. Since the stability analysis is performed in the system of reference with respect to which the travelling waves are stationary, the presence of the finite imaginary part σ_{i} indicates that a time dependence with the frequency $\omega_2 = \omega_1 \pm \sigma_{\mathrm{i}}$ is introduced by the growing instability. The numerical simulation to be reported below shows that the negative sign must be chosen in this relationship.

Because the transition to asymmetric travelling waves is associated with a second frequency, it is in general not possible to find a frame of reference with respect to which the travelling wave becomes stationary. This complication has led us to introduce the representation (2.7) and to solve in a few cases the basic equations by numerical integration in time. Starting from the symmetric-travelling-wave solution as the initial condition with small disturbances of the asymmetric kind superimposed, the solution approaches a state which can be described approximately as the superposition of two travelling waves onto the steady-roll configuration. Because of their opposite symmetry properties the two waves interact mainly through the terms describing the time-independent component of convection. A typical example of this form of time-dependent convection is shown in figure 8. As the two waves propagate along the rolls at different speeds the maximum distortion of the roll occurs alternately on the centre roll and the outer rolls shown in the figure. The two main frequencies, 25.2 and 12.9, exhibited by the asymmetric travelling wave correspond closely to the frequency $\omega_1 = 25.0$ (for $N_{\mathrm{T}} = 7$) of the symmetric travelling wave and to the disturbance frequency $\omega_2 = \omega_1 - \sigma_{\mathrm{i}} \approx 12.8$. A more detailed inspection of the time dependence indicates a tendency towards phase locking which is not surprising

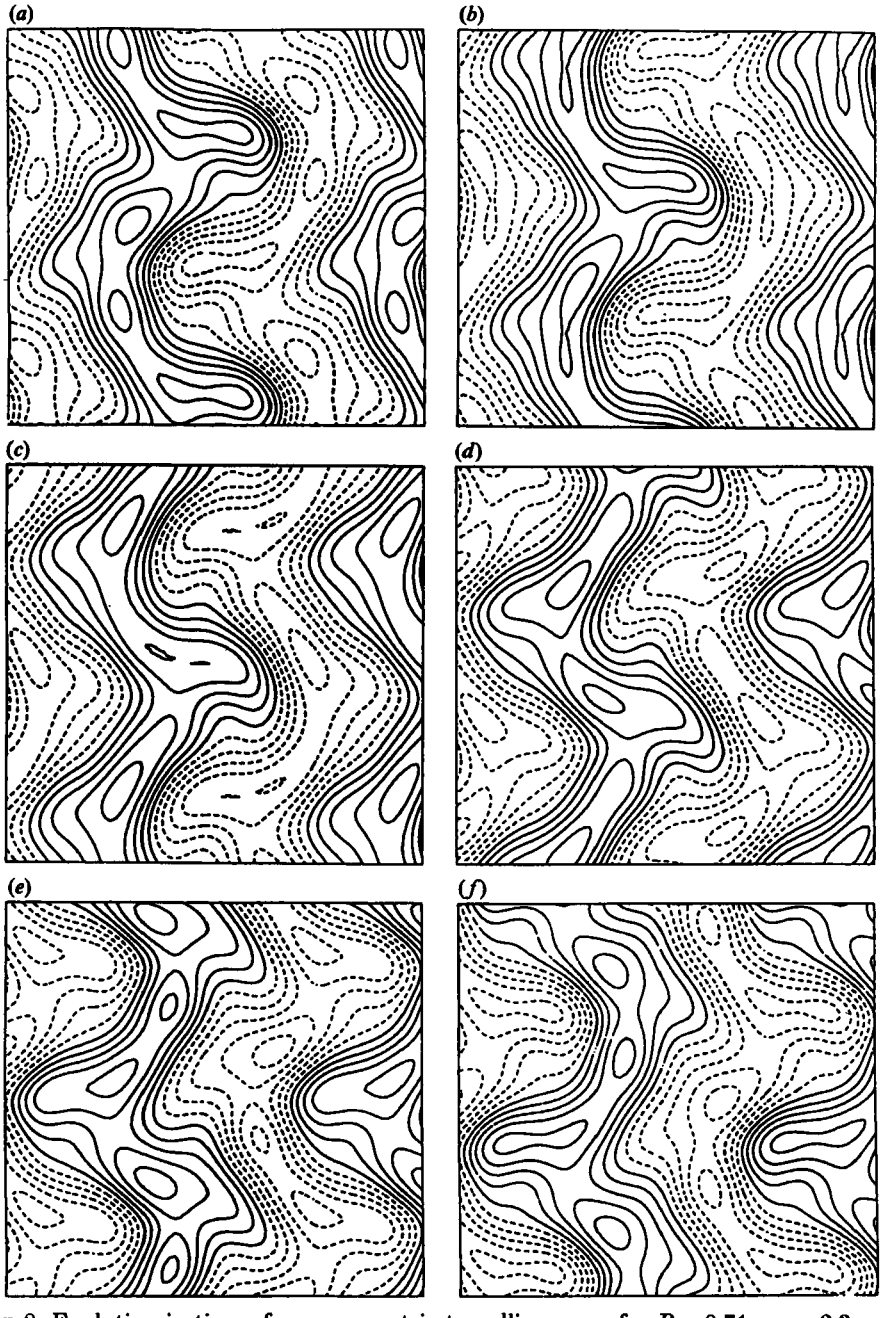

FIGURE 8. Evolution in time of an asymmetric travelling wave for $P = 0.71$, $\alpha_x = 2.3$, $\alpha_y = 2.2$, $R = 10^4$. The plots which show lines of constant vertical velocity in the plane $z = 0$ show a sequence in time from (*a*)–(*f*) with a timestep $\Delta t = 0.05$. The truncation parameter $N_T = 7$ has been used.

in view of the approximate relationship $\omega_1 = 2\omega_2$. But because of the weak phase-dependent part of the interaction between symmetric and asymmetric components of the travelling wave, the phase locking lasts only for about five to ten periods.

The above-developed picture of the asymmetric travelling waves agrees basically with the findings of Lipps (1976) and McLaughlin & Orszag (1982). The shape of the

waves and their two main frequencies are in general agreement if the slight differences in the horizontal wavenumbers are taken into account. The relatively small value of α_y used by Lipps together with the short timespan of his numerical simulation may be responsible for the fact that he did not observe in his run D the periodic shifting of the maximum distortion back and forth between the inner and outer roll as shown in figure 8.

The stability analysis performed by us did not reveal any indication of a weak instability which could be responsible for the high second frequency found by McLaughlin & Orszag (1982) in the frequency spectrum in the regime of symmetric travelling waves. Since the power associated with this second frequency is less than 10^{-5} of the power of the primary frequency the possibility of a numerical effect perhaps cannot be excluded. In their numerical simulation of the asymmetric travelling wave in air at Rayleigh numbers between 9×10^3 and 12×10^3 McLaughlin & Orszag sometimes find a third frequency. This frequency could arise from the weak tendency of the convection to move temporarily into a frequency-locked state.

5. Discussion

The analysis of the preceding sections has in part been motivated by the conflicting claims about the effect of oscillatory convection on the Nusselt number. The theoretical results indicate quite clearly that the onset of travelling waves decreases the efficiency of the convective heat transport. The small decrease in the slope of the Nu–R relationship for air at $R = R_{\mathrm{II}}$ is in agreement with the observation made by Brown (1973), that no significant change in the slope of the experimentally measured Nu–R relationship could be detected at the onset of oscillations. Because the average measured wavenumber α_y decreases with increasing Rayleigh number and because of the three-dimensionality of the experimentally observed convection pattern, the measured values of $Nu-1$ are smaller by about 10 % than the calculated values of table 1. The property that the change in slope increases with decreasing Prandtl number is evident from the measurement of the heat transport in liquid helium (Maeno *et al.* 1985). The changes in slope of opposite sign observed for convection in mercury by Fauve & Libchaber (1981) must thus be explained as a different physical phenomenon. Because of the small width-to-height ratio of the layer used by the latter authors, a rearrangement or change in the number of the convection rolls may well lead to kinks in the Nu–R dependence. Since no significant deviations from the earlier data of Rossby (1969) were seen and since the latter can be well interpreted in terms of the heat transport by travelling waves according to figure 7, there does not seem to be any significant discrepancy between the present theory and the observations by Fauve & Libchaber.

McLaughlin & Orszag (1982) have demonstrated the important role played by the transition to asymmetric travelling waves. The introduction of a second frequency by this transition was found to be the precursor for the onset of chaotic motions in accordance with the Ruelle–Takens scenario. It will be of interest to extend the computations by McLaughlin & Orszag to other Prandtl numbers since these authors studied only the case of air for a special horizontal-periodicity interval. Recently Meneguzzi *et al.* (1985) made some progress in this direction. They obtained chaotic solutions in the case of stress-free boundaries. But in the case of rigid boundaries the aperiodic components of motions always decayed in time. According to the analysis of the present paper the explanation for their result must be sought in the fact that their Rayleigh numbers were chosen below the critical values R_{III} for the onset of asymmetric travelling waves.

REFERENCES

BROWN, W. 1973 Heat-flux transitions at low Rayleigh number. *J. Fluid Mech.* **60**, 539–559.

BUSSE, F. H. 1972 The oscillatory instability of convection rolls in a low Prandtl number fluid. *J. Fluid Mech.* **52**, 97–112.

BUSSE, F. H. & FRICK, H. 1985 Square-pattern convection in fluids with strongly temperature-dependent viscosity. *J. Fluid Mech.* **150**, 451–465.

CHANDRASEKHAR, S. 1961 *Hydrodynamic and Hydromagnetic Stability*. Clarendon.

CLEVER, R. M. & BUSSE, F. H. 1974 Transition to time-dependent convection. *J. Fluid Mech.* **65**, 625–645.

CLEVER, R. M. & BUSSE, F. H. 1978 Large wavelength convection rolls in low Prandtl number fluids. *Z. angew. Math. Phys.* **29**, 711–714.

CLEVER, R. M. & BUSSE, F. H. 1981 Low-Prandtl-number convection in a layer heated from below. *J. Fluid Mech.* **102**, 61–74.

FAUVE, S. & LIBCHABER, A. 1981 Rayleigh–Bénard experiment in a low Prandtl number fluid. In *Chaos and Order in Nature* (ed. H. Haken), pp. 25–35. Springer.

GRÖTZBACH, G. 1982 Direct numerical simulation of laminar and turbulent Bénard convection. *J. Fluid Mech.* **119**, 27–53.

JONES, C. A., MOORE, D. R. & WEISS, N. O. 1976 Axisymmetric convection in a cylinder. *J. Fluid Mech.* **73**, 353–388.

KRISHNAMURTI, R. 1973 Some further studies on the transition to turbulent convection. *J. Fluid Mech.* **60**, 285–303.

LIPPS, F. B. 1976 Numerical simulation of three-dimensional Bénard convection in air. *J. Fluid Mech.* **75**, 113–148.

MCLAUGHLIN, J. B. & ORSZAG, S. A. 1982 Transition from periodic to chaotic thermal convection. *J. Fluid Mech.* **122**, 123–142.

MAENO, Y., HAUCKE, H. & WHEATLEY, J. C. 1985 Transition to oscillatory convection in a ^{3}He–superfluid–^{4}He mixture. *Phys. Rev. Lett.* **54**, 340–342.

MENEGUZZI, M., SULEM, C., SULEM, P. L. & THUAL, O. 1985 Three-dimensional numerical simulation of convection in low-Prandtl-number fluids. *J. Fluid Mech.* (submitted).

ROSSBY, H. T. 1969 A study of Bénard convection with and without rotation. *J. Fluid Mech.* **36**, 309–335.

WILLIS, G. E. & DEARDORFF, J. W. 1970 The oscillatory motions of Rayleigh convection. *J. Fluid Mech.* **44**, 661–672.